ELSEVIER

Polymer 43 (2002) 3779–3784

polymer

www.elsevier.com/locate/polymer

Nanostructure evolution of oriented high-pressure injection-molded poly(ethylene) during heating

Norbert Stribeck[a,*], Rüdiger Bayer[b], Gebhardt von Krosigk[c], Rainer Gehrke[d]

[a]*Institut f. Technische u. Makromolekulare Chemie, Universität Hamburg, Bundesstr. 45, 20146 Hamburg, Germany*
[b]*Institut f. Werkstofftechnik, Universität GH Kassel, Mönchebergstr. 3, 34125 Kassel, Germany*
[c]*FB Physik, Universität Rostock, Universitätsplatz 3, 18051 Rostock, Germany*
[d]*HASYLAB am DESY, Notkestr. 85, 22603 Hamburg, Germany*

Received 15 October 2001; accepted 27 February 2002

Abstract

High-pressure injection-molded polyethylene (PE) rods are studied by ultra small-angle X-ray scattering from synchrotron during the heating of the polymer. Injection of a cool melt into a cold mold yields highly oriented PE rods with a core–shell structure. Samples from both the core and the shell material are studied. The two-dimensional scattering patterns are evaluated utilizing the multi-dimensional chord distribution function (CDF) analysis. From the obvious evolution of the nanostructure during successive crystallite melting, the sequence of processes occurring during crystallization is elucidated. First, nuclei form one-dimensional lattices with short-range order along the fiber axis. From this row structure, lamellae grow with wide lateral extension. An indication of an intermediate block structure is observed. Finally two steps of insertion crystallization result in two long period halvings. Increase of the mold pressure increases the lateral extension of the inserted lamellae in the shell material. In the core material a uniform row structure is absent. Extended primary lamellae form stacks with decreasing long periods before insertion crystallization takes over. But crystallites inserted in the core material do not form extended lamellae. Each of these steps leaves its footprint in the nanostructure and the corresponding scattering pattern. After CDF interpretation of the heating series, the room temperature pattern can be explained. The strong two-point pattern is associated with the primary lamellae and the intensity ridge extending along the meridian results from irregular insertion of lamellae. When the row structure is observed in the CDF, the fiber pattern exhibits equatorial scattering.

Domain roughness generates a strong background scattering, which cannot be separated in one step. For the presented material it is shown that iterative background subtraction eliminates the scattering effects of the imperfect (i.e. inserted) lamellae. © 2002 Published by Elsevier Science Ltd.

Keywords: Ultra small-angle X-ray scattering; Polyethylene; Crystallization and melting

1. Introduction

The determination of nanostructure from small-angle scattering patterns is a matter of constant interest for materials scientists, especially in the field of synthetic polymer materials, many of which are considered two-phase systems. After it was recognized that time-resolved measurement of nanostructure evolution is possible utilizing synchrotron radiation, it took 2 decades of development to supply facilities that meet the requirements of materials science. An example is beamline BW4 of HASYLAB in Hamburg. In 1999, after finally reconstructing the optical system, high quality scattering patterns with fiber symmetry were recorded for the first time. These images demonstrated the complexity of polymer nanostructure and, moreover, the need for advanced data evaluation methods. A method was devised which reduced the problem to one dimension [1]. Its limits were experienced with the data presented here. We felt that the complex models necessary for fitting the data should not be determined by trial and error followed by indirect reasoning. Therefore the method of multi-dimensional chord distribution function (CDF) analysis was developed [2]. The multi-dimensional CDF is the auto-correlation of the gradient of the density in the multi-phase system, which by definition, vanishes everywhere except at the phase boundaries. The CDF permits to directly visualize the domain shapes and their mutual correlation in space in two or three dimensions. Its feasibility has been demonstrated recently [3] for the case of nanostructures built from cylinders or spheres. Now the study of a nanostructure

* Corresponding author. Tel.: +49-40-42838-3615; fax: +49-40-42838-6008.
E-mail address: norbert.stribeck@desy.de (N. Stribeck).

0032-3861/02/$ - see front matter © 2002 Published by Elsevier Science Ltd.
PII: S0032-3861(02)00171-4

is presented that commonly is considered to be built from stacks of crystalline and amorphous lamellae.

The material was prepared by high-pressure injection-molding (HPIM) of a cool melt into a cold mold and we obtained highly oriented polyethylene (PE) rods. Isotropic material is obtained if a hot melt (250 °C) is injected into a hot mold and cooled slowly (1 °C/min). A comprehensive USAXS investigation concerning such material has recently been presented [4]. The complete quantitative analysis of the corresponding extensive data could be managed, because the possibilities of automatization [5] were exploited which became obvious during CDF method development. Then known methods for the analysis of lamellar two-phase systems [6,7] were employed. USAXS analysis revealed a coupled process of melting and crystallization which is not accompanied by external heat flow. It showed that the isotropic high-pressure (280 MPa) materials contain considerable amounts of imperfect thin crystals that melt at lower temperature, while at the same time thick crystallites are formed. With lower pressure samples (210 MPa) the generation of thick lamellae was found to be negligible.

In the investigation presented here we have not performed quantitative analysis of the scattering data. Therefore a question concerning coupled processes of melting and recrystallization are beyond our reach. Here we intend to demonstrate how the multi-dimensional CDF can help to describe the evolution of the nanostructure during melting of the poly(ethylene) and how from the findings conclusions can be drawn concerning the multi-stage crystallization process that determines the fundamental properties of the complex nanostructure of this peculiar material. Because we are utilizing the three-dimensional (3D) CDF we do not need to assume a system of extended lamellae. We can investigate the dimensions of crystals directly—both in fiber and in transversal directions as a function of temperature. When approaching melting temperature, we should be able to answer the question if the last observed discrete SAXS is originating from an ensemble of uncorrelated crystalline lamellae only.

2. Experimental section

High-pressure injection-molded rods from poly(ethylene) (Lupolen 6021 D, BASF) exhibit a core–shell structure (Fig. 1). In order to achieve high orientation, an equilibrated melt of 160 °C was injected into the cold mold. The pressure–time diagram of the molding process is shown in Fig. 2. Maximum mold pressure was 444 MPa and final mold pressure 336 MPa after 180 s. Three more samples with different molding pressure were studied. The lowest maximum mold pressure was 412 MPa. In DSC, all samples exhibit bimodal melting with peak maxima at 131 and 141 °C.

Samples for the USAXS investigation were sectioned from the shell and the core of the rod, respectively, using a low-speed diamond saw.

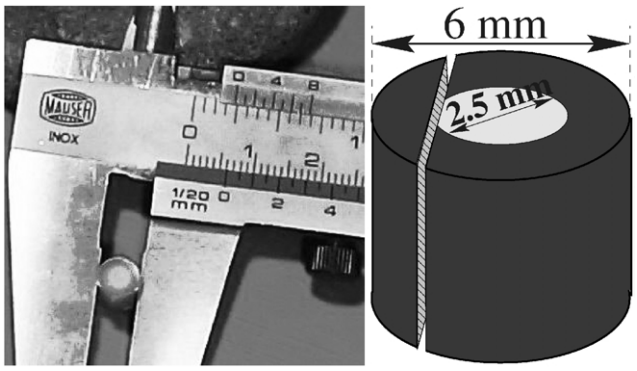

Fig. 1. PE injection-molded rod with core–shell structure and sectioning of a shell sample.

Ultra small-angle X-ray scattering (USAXS) was performed in the synchrotron beamline BW4 at HASYLAB, Hamburg, Germany. The wavelength of the X-ray beam was 0.1366 nm. USAXS images were collected by a two-dimensional (2D) position sensitive Gabriel detector (512 × 512 pixels of $0.4 \times 0.4\ mm^2$) (from European Molecular Biological Laboratory, EMBL). The sample-to-detector distance was set to 12,690 mm. The minimal accessible scattering angle corresponded to a d-spacing of 860 nm. The maximal scattering angle corresponded to 16 nm.

During image collection, each sample was heated from 25 to 150 °C. Below 100 °C a heating rate of 5 °C/min was chosen. Thereafter the heating rate was slowed to 2 °C/min. Images were accumulated for 90 s. Data storing took 30 s.

3. Data evaluation

The 2D scattering patterns were normalized to detector efficiency and incident beam flux. Background subtraction and sample absorption were subsequently operated. Blind areas were masked in the images. Each image was centered and aligned using the positions of the observed two-point patterns. Four-quadrant averaging was carried out. The remnant central blind spot from the beam stop was filled.

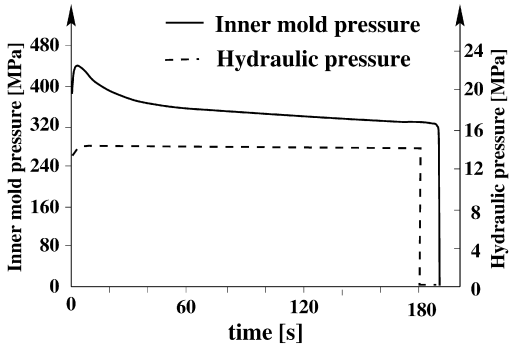

Fig. 2. Pressure–time diagram of the injection molding process.

Data for a smooth extrapolation were supplied by radial basis function approximation [8]. In similar manner, a smooth extrapolation was computed for wider scattering angles. The final scattering patterns covered the range $s_{12}, s_3 \in (-0.072\,\mathrm{nm}^{-1}, +0.072\,\mathrm{nm}^{-1})$ with the modulus of the scattering vector s defined by $s = \sqrt{s_{12}^2 + s_3^2} = (2/\lambda)\sin\theta$ and 2θ being the scattering angle. As described earlier [2] the scattering intensity was projected onto the (s_1, s_3)-plane, multiplied by s^2, then regridded to 512×512 pixels. The 2D background was determined (Butterworth low pass filter of first order with a cut-off frequency $r_c = 1$ in units of pixels) and subtracted. The result was multiplied by the cosine-bell function ('Hann window') and subjected to 2D Fourier transformation in order to obtain the 3D chord distribution $z(\mathbf{r})$.

4. Results and discussion

The USAXS patterns. Fig. 3 exhibits the logarithm of the USAXS intensity from the shell zone of the highest pressure-molded PE rod at specific temperatures during heating of the sample. Data are normalized to primary intensity and machine background is subtracted.

Sharp long period reflections with a peak maximum corresponding to 100 nm are obvious in all patterns. The peaks are placed on top of an intensity ridge extending along the meridian. As a function of increasing temperature, the shape of the ridge is changing, whereas the peak appears to be almost unchanged. The ridge disappears before melting. Early at 128 °C equatorial scattering is indicated. With increasing temperature it becomes more pronounced and vanishes as the last discrete feature when the sample is melting.

Fig. 4 shows the corresponding USAXS from the core zone of the highest pressure-molded PE rod. As compared to the shell zone scattering we observe more diffuse patterns. But the orientation of the core material is obvious, especially in the pattern recorded at 129 °C.

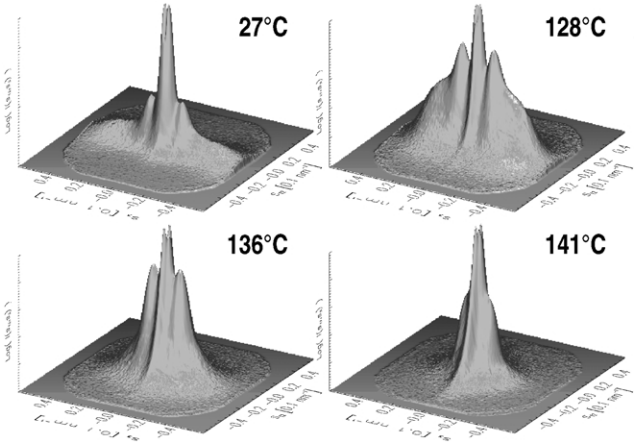

Fig. 3. USAXS intensity log ($I(s)$) from the shell zone of a PE rod at various temperatures during heating.

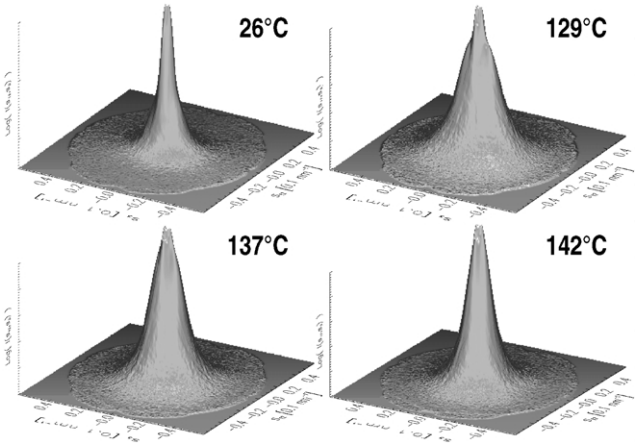

Fig. 4. USAXS intensity log ($I(s)$) from the core zone of a PE rod at various temperatures during heating.

A direct interpretation of these patterns appears to be difficult and ambiguous. In unpublished work we have tried to analyze the intensity projected on to the meridian [1] utilizing the method of interface distribution analysis [6,7]. None of the scattering curves could be fitted by a simple model of lamellae or lamellar stacks, respectively.

3D-Chord distributions of the shell material. Fig. 5 presents 3D CDFs $z(\mathbf{r})$ of the shell material at various temperatures during heating. All plots show the same interval in all three directions.

It is obvious that a lamellar system is present at ambient temperature. Each of the strong, triangle shaped peaks describes both crystalline lamellae and amorphous layers. The corresponding layer thickness distributions are broad and cause the corresponding peaks merge into one. The long period (26 nm) is much smaller than expected from the peak maximum of the scattering pattern.

At 128 °C peak heights have grown. The reason is different thermal expansion of crystalline and amorphous

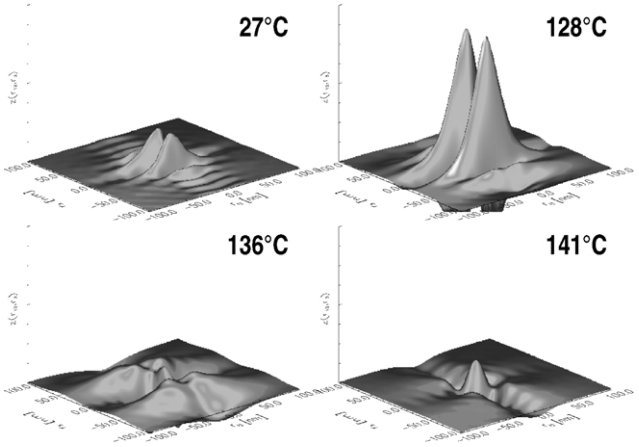

Fig. 5. Shell zone of the PE rod: 3D chord distributions with fiber symmetry, $z(\mathbf{r})$ as a function of temperature during heating in the range $r_{12}, r_3 \in (-100\,\mathrm{nm}, 100\,\mathrm{nm})$.

phases, respectively. From the width of the triangles, an average lateral extension of 70 nm is determined. The undulation frequency in front of the strong peaks has halved just as the temperature of 128 °C has been reached. Thus the long period now has doubled. In the center of the lower peaks of second order an indentation is observed, which is still unexplained at this temperature.

At 136 °C the first minimum in the CDF in meridional direction (i.e. the long period) is found at 95 nm. The imperfect layers have melted and the only observable feature is the layer stack corresponding to the strong peaks in the scattering pattern. The distribution of layer thicknesses is still very broad. The indentation from the last pattern has increased to form a trough extending along the meridian.

At 141 °C the trough has engraved itself to from a deep valley on the meridian. A more shallow, modulated valley is extending along the equator of the CDF. Single lamellae with a very broad thickness distribution are indicated by the low hills in the pattern.

Minima in the valleys are associated to long periods [2]. Fig. 6 shows the contours of the long periods as a function of temperature. It is observed that the long period doubles first at 128 °C and a second time at 136 °C. But still the long equatorial streak indicates the autocorrelation of a lamellar system. At 141 °C the nanostructure has changed fundamentally. The streak at the equator has shrunk to indicate the predominance of domains which are narrow in lateral direction ('blocks'). On the meridian a row of crystal nuclei is observed that form a distorted one-dimensional lattice with a long period of 95 nm. The long period structure is best viewed in a 3D presentation of the CDF turned upside down (Fig. 7). On the meridian, broad but regular long period reflections with narrow lateral extension are

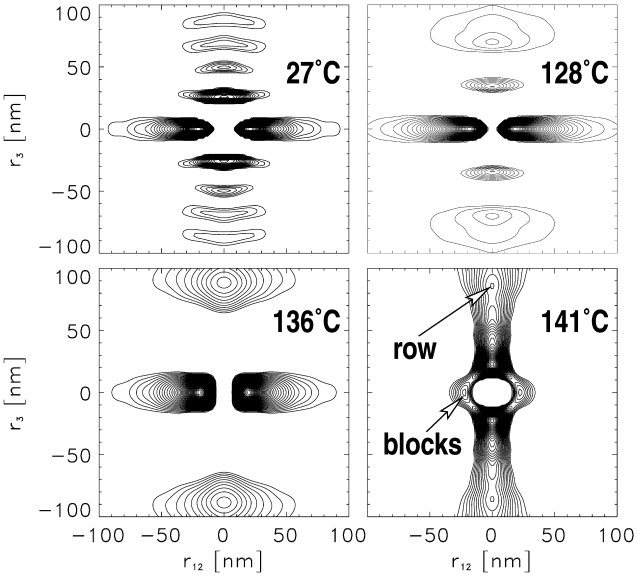

Fig. 6. Shell zone of the PE rod: 3D chord distributions with fiber symmetry, $-z(\mathbf{r})$ as a function of temperature during heating in the range $r_{12}, r_3 \in (-100\text{ nm}, 100\text{ nm})$.

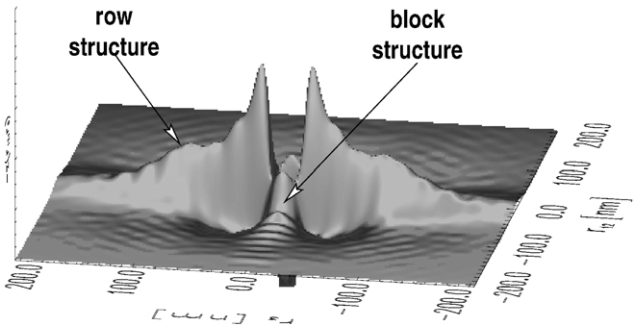

Fig. 7. $-z(\mathbf{r})$ (CDF) of the PE shell material at 141 °C.

observed. The arrow points at the first order of the lattice. The superposed weak modulation is continued over the whole area of the (r_{12}, r_3)-plane and is an artefact (caused from a remnant small step at the edge of the sensitive plane of the detector). At the equator the main modulation is somewhat stronger. If we agree to attach some importance to this observation, it is supporting the notion of Strobl [9–12] according to which crystalline lamellae are generated from a planar arrangement of blocks.

Based on these observations, it appears to be justified to assume, to a first approximation, that during heating those crystallites melt, which were formed last during crystallization. So let us imagine to revert time and to discuss the observed process in terms of a crystallization. Doing so permits to proceed from the simple to the complex nanostructure. Under this premise the results reveal that upon the start of crystallization tiny nuclei form row structures along fiber direction. From these nuclei lamellae grow in lateral direction. The thicknesses of these lamellae are not uniform (20–60 nm). This result may be caused from the fact that the irradiated volume integrates over the total thickness of the shell zone. During the course of cooling new and thin crystal layers are generated somewhere in between the primary lamellae. When the material is cooled even further, the long period is halved a second time. All the time the most regular period is constant and imprinted by the average distance of the nuclei in the rows. This causes the point-shaped long period reflections in the scattering pattern. The subdivision of the primary long period in the subsequent insertion crystallization is highly irregular and generates the intensity ridge extending along the meridian. The strength of the equatorial streak is correlated with the strength of the row structure. Thus the CDF analysis reveals that for the studied materials the insertion model of crystallization [13,14] is more probable than the two-stack model [15]. While the scattering pattern emphasizes the harmonic components of the structure, the CDF shows all the regular and irregular components with equal weight and the complexity of the nanostructure is revealed.

Iterated CDFs. In the paper proposing the CDF method [2] a possibility is discussed to remove strong background scattering by iterating the steps of low-pass filter and background subtraction until the values of the CDF vanish in the

vicinity of zero ('CDF of the second kind'). Domain roughness [16,17] can be compensated this way, but information concerning domain structure may be lost. From all scattering patterns of the shell material, iterated CDFs have been computed and compared to the non-iterated ones. The iterated CDFs reproduce the information concerning the fairly well ordered row structure and the primary lamellae without distortion. Nevertheless, information concerning the imperfect secondary lamellae is lost.

3D-CDF analysis of the core material. Non-iterated CDFs from the core zone of the highest pressure-molded PE rod are shown in Fig. 8. The nanostructure, in general, exhibits less order as compared to the shell material. At room temperature the long periods are small again and the average extension of the crystallites in lateral direction is very small as compared to the shell material. A fingerprint of a row structure is not found. At 124 °C the typical triangular peaks from lamellae with some lateral extensions are seen. Nevertheless, there are still many irregular domains which are not extended in lateral direction. At 129 °C it is observed that the average thickness of the remnant lamellae has increased. At 137 °C only a very broad distribution of the currently extended lamellae is seen. These findings indicate that even in the core material the insertion model of crystallization is preferable. The question concerning the existence of a row structure in the core material cannot be answered from the non-iterated CDFs.

Fig. 9 shows contour plots of the long periods from iterated CDFs. In contrast to the non-iterated CDFs, the iterated CDFs exhibit clear long period reflections. At room temperature the long period is 95 nm which is the value of the row structure period known from the shell material. Unlike the finding with the shell material, this long period first increases slowly (105 nm at 129 °C), then accelerated up to a value of 140 nm at 137 °C. At higher temperature a regular long period cannot be detected any more.

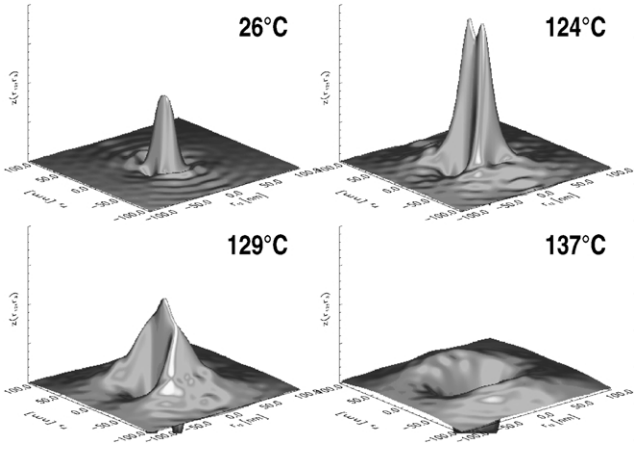

Fig. 8. Core zone of the PE rod: 3D chord distributions with fiber symmetry, $z(\mathbf{r})$ as a function of temperature during heating in the range $r_{12}, r_3 \in (-100\,\text{nm}, 100\,\text{nm})$.

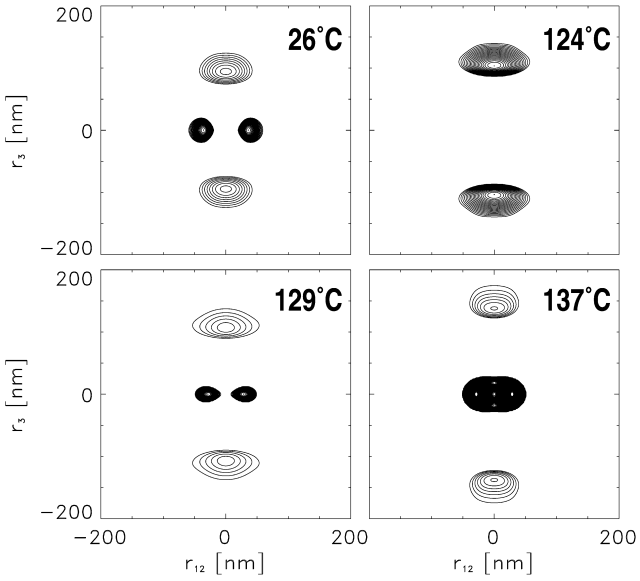

Fig. 9. Core zone of the PE rod: 3D chord distributions with fiber symmetry, $-z(\mathbf{r})$ (iterated) as a function of temperature during heating in the range $r_{12}, r_3 \in (-200\,\text{nm}, 200\,\text{nm})$.

Obviously the lateral extensions of the domains in the core is lower than that in the shell. While the lamellae from the shell exhibit an average cross section of 70 nm, corresponding cross sections in the core material are found between 40 and 60 nm.

In summary, even if the ordered structure of both the shell and the core material show the same long period at room temperature, the nucleation process is different. In the core material the frame of a uniform row structure is missing. On the other hand, insertion crystallization is common during the second stage of crystallization in both the core and the shell material.

Samples prepared at lower pressure. HPIM samples prepared at lower pressure in principle show similar results as the sample discussed extensively. The row structure long period of the shell materials does not change significantly. But the lateral extension of secondary lamellae inserted in the shell material is lower for materials prepared at lower injection pressure.

Comparison to isotropic HPIM material. Compared to the isotropic HPIM materials prepared in a previous study [4] one common feature is found. Both kinds of materials contain a considerable fraction of small crystallites which melt early at low temperature. Poor order of layer arrangement appears to be a typical feature of the isotropic materials, whereas the shell zones of the anisotropic materials exhibit some mid-range order imprinted by an unchanging row structure.

5. Conclusions

Multi-dimensional CDF analysis of the SAXS and

USAXS patterns from oriented samples provides a novel method to study nanostructure in physical space. Global evaluation parameters can be adjusted for a specific setup and complete sample series. Thereafter the algorithms perform automatically. Interpretation of the CDF exhibits a detailed view of nanoscale domain shapes and domain arrangement in space in a presentation that does not emphasize the harmonic fractions of nanostructure.

We have exemplified how this method can be utilized to analyze time-resolved studies of nanostructure evolution in materials science. In similar manner, insight can be gained concerning nanostructure evolution as a function of different kind of material load. From the nanostructure at ambient temperature and the melting behavior of the material, conclusions can be drawn on processes dominating the preceding crystallization.

An interesting finding concerning the high-pressure injection-molded materials is the fact that both the isotropic and the anisotropic materials exhibit a sparsely filled basic domain structure, which in a second process is filled with imperfect crystallites. Neither cooling rate nor melt viscosity appear to influence this basic structural property. We expect that similar investigations will contribute to a deeper understanding of the structure–property relations of polymers and, finally, to the engineering of tailored polymer materials.

Acknowledgements

This study was supported by HASYLAB, Hamburg, project II-98-067.

References

[1] Stribeck N. ACS Symp Ser 2000;739:41–56.
[2] Stribeck N. J Appl Crystallogr 2001;34:496–503.
[3] Stribeck N, Buzdugan E, Serban S, Gehrke R. Submitted for publication.
[4] Wang Z, Hsiao BS, Stribeck N. Submitted for publication.
[5] Stribeck N. Colloid Polym Sci 2002, in press.
[6] Ruland W. Colloid Polym Sci 1977;255(5):417–27.
[7] Stribeck N. Colloid Polym Sci 1993;271(11):1007–23.
[8] Buhmann MD. Acta Numer 2000;9:1–38.
[9] Hugel T, Strobl G, Thomann R. Acta Polym 1999;50:214–7.
[10] Heck B, Hugel T, Iijima M, Sadiku E, Strobl G. New J Phys 1999;1:171–1729.
[11] Iijima M, Strobl G. Macromolecules 2000;33:5204–14.
[12] Heck B, Hugel T, Iijima M, Strobl G. Polymer 2000;41(25):8839–48.
[13] Wang J, Alvarez M, Zhang W, Wu Z, Li Y, Chu B. Macromolecules 1992;25:6943–51.
[14] Hsiao BS, Gardner KH, Wu DQ, Chu B. Polymer 1993;34(19):3996–4003.
[15] Bassett DC, Olley RH, Al Raheil IAM. Polymer 1988;29:1745–54.
[16] Ruland W. Macromolecules 1987;20:87–93.
[17] Wolff T, Burger C, Ruland W. Macromolecules 1994;27(12):3301–9.